A Simple Lagrangian PDF Model for Wall-Bounded Turbulent Flows

Changhoon Lee*, Byunggu Kim
Department of Mechanical Engineering, University of Seoul
Namhyun Kim
Department of Applied Mathematics, Hongik University

A simple Lagrangian pdf model is proposed with a new numerical algorithm for application in wall-bounded turbulent flows. To investigate the performance of the Lagrangian model, we minimize model's dependence on empirical constants by selecting the simplest model for turbulent dissipation rate. The effect of viscosity is also included by adding a Brownian random walk calculate the position of a particle. For the no-slip condition at the wall and correct near-wall behavior of velocity, we develop a new boundary treatment for the particles that strike the wall. By applying the model to a fully developed turbulent channel flow at low Reynolds number, we investigate the model's performance through comparison with direct numerical simulation result.

Key Words : Lagrangian PDF Model, Brownian Motion, Turbulence Model, Wall-Bounded Turbulence

1. Introduction

Since van Dop et al. (1985) proposed a random walk model for calculations of turbulent flows for the first time, a few researchers has been investigating the feasibility of random walk models as turbulence models. Specially, Pope and his co-workers have developed, improved and applied the random walk model, also known as the Lagrangian probability density function(PDF) model, to turbulent reactive flows (Pope, 1985; Howarth & Pope, 1986; Pope & Chen, 1990; Dreeben & Pope, 1997). Lagrangian models are more comprehensive than the classical models derived from the Reynolds averaging process, and the models can treat the nonlinear reaction source terms without approximation. Their application ranges broadly to from shear flows, jet flows to channel flows. Although Lagrangian models are continuously improved for better performance, they have not been widely used in turbulence model development or application studies.

From the viewpoint of turbulence model, Lagrangian models have a major advantage over traditional one-point closure models such as the k-ε model or Reynolds Stress Transport Model. Absence of the nonlinear advection terms in the evolution equation of a Lagrangian particle eliminates the uncertainty associated with a gradient-diffusion modeling of the higher-order correlation terms constantly appearing in the equations for the lower-order correlation. Thus, the model target in Lagrangian models is limited to the pressure strain correlations. Also, a Lagrangian PDF model can provide many Lagrangian statistical turbulence data which cannot be easily obtained from Eulerian turbulence models. Probability density functions and Lagrangian velocity structure functions or higher-order correlations are examples. These will give us some insight into the flow structures in question.

* Corresponding Author,
E-Mail : chlee@seoul.uos.ac.kr
TEL +82-2-2210-2603 ; **FAX** : +82-2-2248-5110
Department of Mechanical Engineering, University of Seoul, 90, Jeonnong-dong, Dongdaemun-ku, Seoul 130-743, Korea.(Manuscript **Received** March 31, 2000; **Revised** May 24, 2000)

From the numerical point of view, a Lagrangian model is superior to other models adopting the Eulerian approach. A Lagrangian model does not require a physical grid system to obtain the Eulerian data; thus numerical difficulties associated with typical temporal integration of an evolution equation in the grid system such as the restriction on the time step due to the CFL condition do not occur. Also, the computational burden increasing with the Reynolds number is less severe than typical numerical scheme adopting the Eulerian approach for the same reason.

One important merit of the Lagrangian approach is that a Lagrangian model not only calculates the flow variables such as velocity, but also provides information about particle dispersion because the model directly computes particle trajectories. So it is a good methodology to compute diffusion as well as a turbulence model. Therefore, the Lagrangian approach is ideal for pollutant dispersion studies.

Recently, the effect of viscosity has been incorporated into the Lagrangian model by Dreeben & Pope (1998). Their idea is similar to that of Chorin(1975) and derives a numerical scheme for the random vortex method. From the characteristics of the viscous diffusion, they added Brownian motion to the calculation of trajectory of a particle. For the no-slip condition at the wall, they proposed a particle collision model. With a modification of the model utilizing an anisotropic representation of the Reynolds stress model of Durbin(1993), they simulated a turbulent channel flow. Their derivation, however, is based on the Langevin model derived from Kolmogorov's scaling assumption of the Lagrangian velocity structure function in the inertial range for homogeneous turbulence. Because of scale disparity between the inertial range and viscous dissipation range, justification of the addition of the Brownian walk model to the turbulence model derived from the inertial range scaling should be carefully examined. Minier & Pozorski(1997) derived the same pdf model using principles from statistical physics, but their model is consistent with Kolmogorov's hypothesis for the inertial range. Consequences of the Lagrangian model including the viscous effect in the viscous time and length scales need to be investigated.

In this paper, our purpose is two-fold: First, we investigate feasibility as a turbulence model of the Lagrangian model with the viscous effect in calculating highly anisotropic flows. We develop a numerical algorithm that computes the velocities and positions of particles using the simple Langevin model with the viscous effect included. Importance of the wall boundary treatment to satisfy the no-slip condition in the Lagrangian approach is carefully investigated since the boundary condition sensitively influences not only near-wall turbulence but also the flow field far from the wall. Some proposed new boundary treatments in the log-law region so that they can avoid resolving problem in the viscous sublayer (Dreeben & Pope, 1997; Minier & Pozorski, 1999). These treatments, however, introduce uncertainty into the model, thus causes the model to be more unreliable. Second, since a Lagrangian method can provide Lagrangian turbulence data, the effect of viscosity in the Lagrangian structure function or correlations is discussed. In particular, the performance of the model in the viscous time scale and probability density functions are examined in detail.

This paper is organized as follows: The governing equations for the Lagrangian velocity and position of a particle is described in Sec. 2. The numerical schemes for time integration and averaging are introduced in Sec. 3. Section 4 explains the model test results for a turbulent channel flow. Section 5 concludes our study. Appendices include detailed explanations of the integration scheme and kernel regression.

2. Governing Equations

There are two derivations of the evolution equation of the Lagrangian velocity-one using the Langevin equation with Kolmogorov's hypothesis by Pope(1994) and the other using a principle from statistical physics by Minier & Pozorski(1997). In this paper we follow Pope's derivation although the original idea dates back to van Dop et al. (1985). For high Reynolds

number homogeneous flows, from Kolmogorov's hypothesis the Lagrangian velocity structure function $D_L(\tau)$ defined by

$$D_L(\tau)\equiv<(U(t+\tau)-U(t))^2> \quad (1)$$

can be scaled in the inertial range as(Monin & Yaglom 1975)

$$D_L(\tau)=C_0\epsilon\tau \quad \text{when } \tau\gg\tau_\eta \quad (2)$$

where the bracket denotes averaging over samples and $U(t)$, C_0, ϵ are Lagrangian velocity, Kolmogorov's constant and mean dissipation rate, respectively. τ_η is the Kolmogorov time scale, $(\nu/\epsilon)^{1/2}$. Equation. (2) indicates that the Lagrangian velocity increment can be modeled as a Gaussian random variable with mean zero and variance proportional to τ. A stochastic differential equation with such properties is the well-known Langevin equation:

$$dU(t)=-\frac{U(t)}{T_L}dt+\frac{\sqrt{2u'^2}}{T_L}dW(t) \quad (3)$$

where $W(t)$ is a Wiener process such that $dW(t)$ is a Gaussian random variable with zero mean and variance dt. This equation describes a Markov process, thus $U(t+dt)$ is determined independently of how $U(t)$ was determined. T_L and u'^2 are the Lagrangian integral time scale and variance of U, respectively. The Langevin equation yields the structure function:

$$D^L(\tau)=\frac{2u'^2}{T_L}\tau \quad (4)$$

when $\tau/T_L\ll 1$. Comparison of Eqs. (2) and (4) yields:

$$\frac{1}{T_L}=\frac{C_0\epsilon}{2u'^2}=\frac{3}{4}C_0\frac{\epsilon}{k}, \quad (5)$$

where k is the turbulent kinetic energy and an isotropic relation between u'^2 and k was used. With this expression for T_L, the Langevin equation (Eq. (3)) can be written as:

$$dU(t)=-\frac{3}{4}C_0\frac{\epsilon}{k}U(t)dt+\sqrt{C_0\epsilon}dW(t). \quad (6)$$

Now, we consider extension of the Langevin equation for application to inhomogeneous flows at finite Reynolds numbers. We make three modifications to Eq. (6). First, consider the case with a mean Eulerian velocity component. Then the fluid particle velocity relaxes to the Eulerian mean. Second, the coefficient of the drift term is modified such that the process correctly represents a dissipating system since Eq. (6) describes a stationary, Gaussian, Markov process known as *the Ornstein Uhlenbeck (OU) process*. With these two modifications, Eq. (6) for each component can be rewritten as:

$$dU_i(t)=-\left(\frac{1}{2}+\frac{3}{4}C_0\right)\frac{\epsilon}{k}(U_i(t) -<u_i>)dt+\sqrt{C_0\epsilon}dW_i(t) \quad (7)$$

where $<u_i>$ is the Eulerian mean velocity and $W_i(t)$ are three independent Wiener processes with zero mean and covariance

$$<dW_idW_j>=dt\delta_{ij}. \quad (8)$$

The coefficient 1/2 in the drift term represents the viscous dissipation effect and correctly causes the turbulent kinetic energy to be dissipated at the rate ϵ. Equation (7) can be thought of as the governing equation for the Lagrangian velocity increment for an infinite Reynolds number flow with dissipation in the absence of a mean pressure gradient.

The third modification to include the effects of a mean pressure gradient and viscosity requires a lengthy derivation. In order to include the viscous effect, we consider a fluid particle motion $X_i(t)$. Since the viscous diffusion can be modeled by Brownian motion, the equation for a particle's displacement can be written as:

$$dX_i=U_idt+\sqrt{2\nu}dW_i \quad (9)$$

where ν is viscosity and W_i is a Wiener process independent from Eq. (8). On the other hand, Lagrangian velocity increment dU can be expressed in terms of Eulerian velocity $u_i(x_i, t)$ using the Taylor expansion. Up to the second-order terms,

$$dU_i=\frac{\partial u_i}{\partial t}dt+\frac{\partial u_i}{\partial x_j}dX_j+\frac{1}{2}\frac{\partial^2 u_i}{\partial x_j\partial x_k}dX_jdX_k \quad (10)$$

where x_i denotes the Eulerian coordinates. Substituting Eq. (9) into Eq. (10), neglecting the higher order terms than dt, and using the Navier-Stokes equation yield,

$$dU_i=\left(\frac{1}{\rho}\frac{\partial P}{\partial x_i}+2\nu\frac{\partial^2 u_i}{\partial x_j\partial x_j}\right)dt+\sqrt{2\nu}\frac{\partial u_i}{\partial x_j}dW_j$$

(11)

where dW_j is the increment of the same Wiener process as in the Eq. (9). This equation describes an evolution equation for the Lagrangian velocity increment for laminar flow. For turbulent flows, decomposition of the Eulerian variables into mean and disturbances modifies Eq. (11) as:

$$\begin{aligned} dU_i=&\left(\frac{1}{\rho}\frac{\partial<P>}{\partial x_i}+2\nu\frac{\partial^2<u_i>}{\partial x_j\partial x_j}\right)dt \\ &+\sqrt{2\nu}\frac{\partial<u_i>}{\partial x_j}dW_j \\ &+\left(\frac{1}{\rho}\frac{\partial p}{\partial x_i}+2\nu\frac{\partial^2 u_i'}{\partial x_j\partial x_j}\right)dt \\ &+\sqrt{2\nu}\frac{\partial u_i'}{\partial x_j}dW_j \end{aligned} \tag{12}$$

where p and u_i' denote disturbances of pressure and velocities. Disturbance parts, in the third and fourth line of the equation, which represent fluctuations in pressure and viscous dissipation, require a turbulence model and can be replaced by the right-hand side of Eq. (7) yielding,

$$\begin{aligned} dU_i=&\left(\frac{1}{\rho}\frac{\partial<P>}{\partial x_i}+2\nu\frac{\partial^2<u_i>}{\partial x_j\partial x_j}\right)dt \\ &+\sqrt{2\nu}\frac{\partial<u_i>}{\partial x_j}dW_j \\ &-\left(\frac{1}{2}+\frac{3}{4}C_0\right)\frac{\epsilon}{k}(U_i-<u_i>)dt \\ &+\sqrt{C_0\epsilon}dW_i' \end{aligned} \tag{13}$$

where W_i' is a Wiener process independent from W_i. This completes modifications to the Langevin equation.

Usually, solving the stochastic differential equation Eq. (13) for velocity and Eq. (9) for particle displacements for a great number of randomly distributed particles constitutes a Lagrangian pdf modeling since it is equivalent to solving an evolution equation for the Lagrangian joint pdf known as the Fokker-Planck equation. Interested reader should refer to Pope (1985) or Gardiner (1997).

In order to solve Eqs. (9, 13) numerically, information on dissipation rate, $\epsilon(x_i,t)$, is required. Pope & Chen (1990) derived a stochastic differential equation for turbulent frequency ω $(x_i,\ t)(\equiv\epsilon(x_i,t)/k(x_i,t))$ using the log-normal property of the probability density function of epsilon for homogeneous turbulence. In the present study, we did not adopt this model because the model's several empirical model constants increase the model's uncertainty and do not complete near-wall modification is not complete. Instead, we use a simple model for the dissipation rate derived from a dimensional argument for homogeneous flows,

$$\epsilon(x_i,\ t)=C_l\frac{k^{3/2}}{l} \tag{14}$$

where l is a length scale proportional to the mixing length and C_l is a model constant that can be estimated from the near-wall equilibrium condition. For application to near-wall flows, a Van Driest type mixing length model is selected,

$$l=C_l^{1/4}\kappa y\left(1-\exp\left(-\frac{yu_\tau}{\nu A}\right)\right) \tag{15}$$

where κ, y, u_τ and A are the von Karman constant, distance from the wall, wall-shear velocity and a model constant. Their values are $C_0=2.5$, $C_l=0.09$, $\kappa=0.41$, and $A=26$. This completes derivation of the simplest stochastic differential equation model for wall-bounded turbulent flows.

3. Numerical Algorithm

3.1 Integration scheme

Equations (9) (13) can be generally written into the following form:

$$\begin{aligned} df(x_i,\ t)=&a(x_i,\ t)fdt+g(x_i,\ t)dt \\ &+h(x_i,\ t,\ f)dW \end{aligned} \tag{16}$$

where the term with an explicit dependence on f is separately shown as in the first term on the right-hand side. A major difference from typical evolution equations is that it has a term, whose magnitude is proportional to $\sqrt{dt}$. Thus, the equation has two levels of dependence on the time step. Integration of the last term is performed using Ito's formulation. Stratonovich's formulation is more difficult to apply due to its semi-implicit nature. For difference between the two formulations, see Gardiner(1997). Equation (16) is numerically solved using a low-storage 3rd-order Runge-Kutta scheme with an exact treatment of the first term. The exact treatment of the

first term is inevitable since a can assume an unbounded value near the solid wall boundary. Detailed expression of the integration scheme can be found in Appendix A.

3.2 Kernel regression

Integrations of Eqs. (9, 13) does not require a physical grid system since it solves for evolution of each particle independently. The coefficients of the evolution equation, however, include information on Eulerian variables such as velocity, pressure, and dissipation rate. Therefore, we need to extract the Eulerian information from distributed particle information. For such a purpose, we adopt a kernel regression (Hardle 1990). As a fitting function, we select a polynomial:

$$\tilde{f}(y-y_j)=\sum_{k=0}^{K} c_k(y-y_j)^k \tag{17}$$

where y, y_j and K are the space variable, particle location, and order of approximation, respectively. This fitting function not only computes regression of the approximated function but also provides derivatives up to K-th order. However, application of this kernel regression for every particle requires a significant amount of computation time. Thus, collocation points are selected and the Eulerian means are computed at these points. Then interpolation is carried out to compute the mean value at the particle location. Details are found in Appendix B.

3.3 Boundary conditions

No-slip boundary condition at solid walls should be satisfied in the evolution of Lagrangian particle velocity when viscous effect is considered. Enforcement of the no-slip condition can be made by modifying the velocities of the particles that strike the wall. With y denoting the wall -normal coordinate, new position of a particle strikes the wall is given as:

$$y_{new}^{n+1}=|\,y^{n+1}\,| \quad if \quad y^{n+1}<0 \tag{18}$$

where y^{n+1} is $n+1$st time step position of a particle computed from Eq. (9). Even when $y^{n+1}>0$, a particle can have a path with $y<0$ during the period Δt since near the wall particle trajectory is well approximated by Brownian motion due to viscosity. Such probability is easily obtained (Dreeben & Pope 1998, Karatzas &

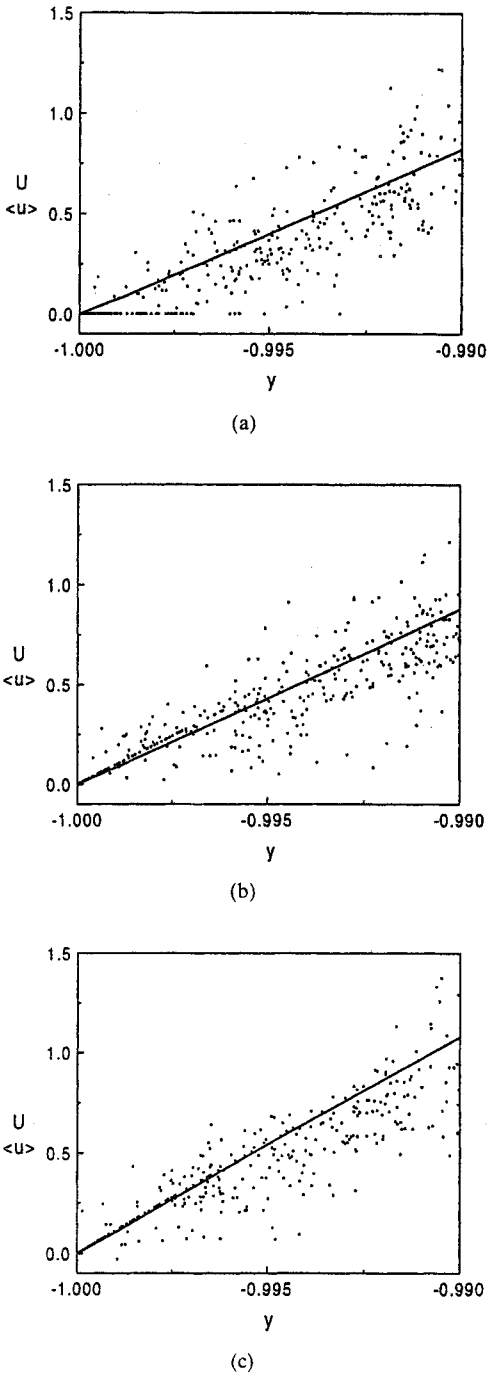

Fig. 1 Near-wall particle velocities for three boundary treatments: (a) type A(Eq. 20); (b) type B (Eq. 21); (c) type C (Eq. 22). All quantities are nondimensionalized u_τ and h

Shreve 1991):

$$prob.(y(t)<0 \mid t^n<t<t^{n+1})=\exp\left(-\frac{y^n y^{n+1}}{\nu\Delta t}\right). \tag{19}$$

In either case, the velocity of the particle is modified to enforce the no-slip condition. Three treatments are considered:

$$A)\ U_i^{n+1}=0 \tag{20}$$

$$B)\ U_i^{n+1}=y_{new}\frac{\partial<u_i^n>}{\partial y}\bigg|_{y=0} \tag{21}$$

$$C)\ U_i^{n+1}=y_{new}\frac{\partial<u_i^n>}{\partial y}\bigg|_{y=0}+\frac{1}{2}y_{new}^2\frac{\partial^2<u_i^n>}{\partial y^2}\bigg|_{y=0} \tag{22}$$

where type A prescribes zero velocity for a particle that strikes the wall and types B and C make use of the first-order and second-order Taylor expansion at the wall, respectively. These three treatments are tested in a turbulent channel flow and the near-wall particle velocities are demonstrated in Fig. 1. Throughout the paper, all of the quantities in figures are nondimensionalized by the wall-shear velocity u_τ and the channel half gap h. As expected, type A underestimates the particle velocity near the wall and in the rest of the channel. Specially, a large discrepancy between the particle velocity and the Eulerian mean velocity is observed in the region very close to the wall when compared to types B and C.

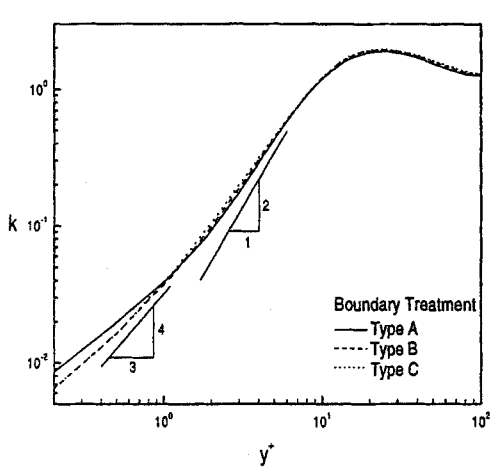

Fig. 2 Near-wall behavior of the turbulent kinetic energy for three boundary treatments

Note the particle velocities along a line element near the wall due to each type of boundary treatment. The near-wall behavior of turbulent kinetic energy, a measure of variance of the particle velocity, is shown in Fig. 2. Types B and C cause the variance to decay faster than type A with the distance from the wall going to zero although the limiting slope does not reach 2. From this test, we find that type C produces the best result. Also, convergence performance of the mean velocity calculation using type C boundary treatment is the best among three. Therefore, we adopt type C boundary treatment in all of our computations.

4. Test Results

The numerical algorithm explained in the previous section is tested in simulations of a fully developed turbulent channel flow subject to a constant pressure gradient. The Reynolds number based on the wall shear velocity u_τ, the channel half gap h, and viscosity is 100. The reason we choose this flow as our test case is that the flow is marginally turbulent, thus the effect of viscosity is maximized and the walls play important roles in determining flow characteristics. Therefore, we can test how the Lagrangian model, derived from Kolmogorov scaling for high Reynolds number isotropic turbulence, performs in an anisotropic low Reynolds number flow. Also, there is direct numerical simulation (DNS) result for this case. Thus, performance test can be made through comparison. Initially, we distribute 32,000 particles randomly throughout the channel and let these particle evolve according to Eqs. (9, 13). 65 nonuniform grids are selected in the wall-normal direction using the cosine function in order to capture steep variations of the Eulerian mean values of velocity and turbulence quantities. This facilitates comparison with the DNS results.

4.1 Global performances

In this section, we investigate the current model's global performance such as distributions of the mean velocity, turbulence intensity, etc. Figures 3(a) and 3(b) show mean streamwise velocities(compared with DNS results) (Kim et

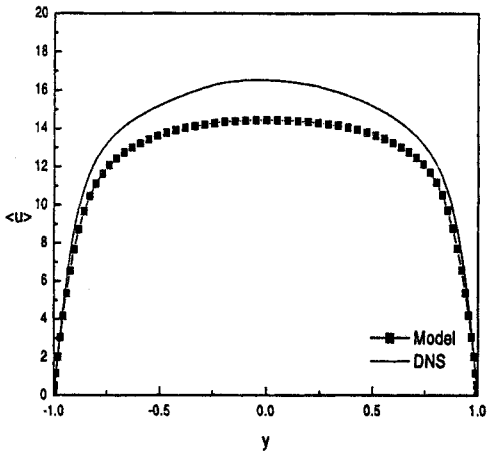

(a)

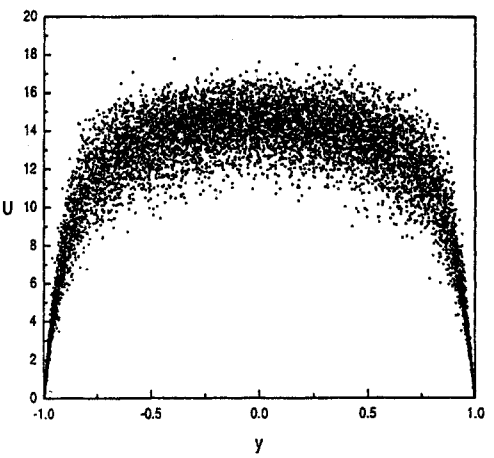

(b)

Fig. 3 (a) Mean Eulerian velocity and (b) Lagrangian particle velocities in a fully developed channel flow

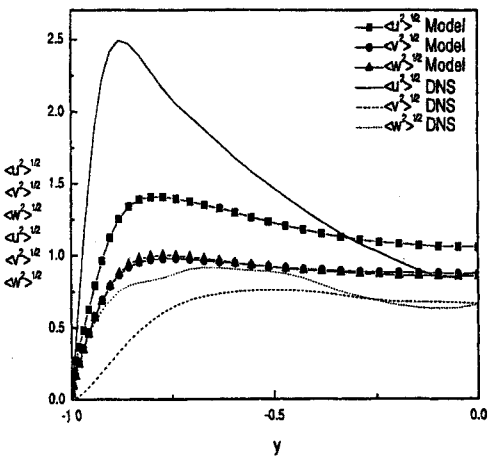

Fig. 4 Distribution of turbulence intensity DNS results are shown also for comparison

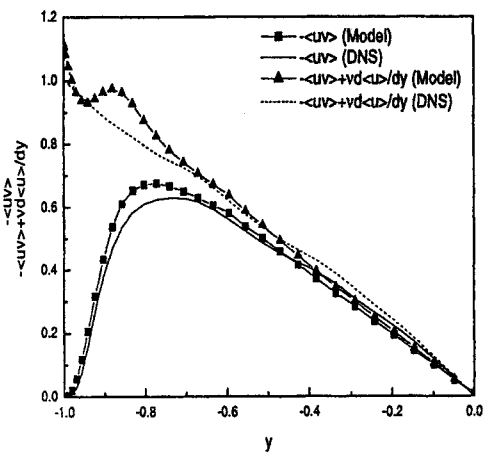

Fig. 5 The Reynolds shear stress and total stress with DNS results

al. 1987, Lee et al. 1997) and Lagrangian particle velocities, respectively. A typical distribution of mean velocity in the channel is simulated by the model, but the model underestimates the mean velocity throughout the channel. Turbulence intensities are displayed in Fig. 4. Near-wall anisotropy is not reflected in our model. Thus, the model does not distinguish between wall normal and spanwise velocities, resulting in identical distributions of the root-mean-squared velocity. The model overestimates the wall-normal and spanwise rms quantities, while underestimating the streamwise rms velocity, which is another symptom associated with the model's inability to capture a strong anisotropy.

The Reynolds shear stress distribution is shown in Fig. 5 along with the total stress which is the sum of the Reynolds shear stress and viscous stress. The total stress is a good indicator of the model's performance. Considering that our model is the simplest Lagrangian model with a minimum number of empirical constants, the model performs well. Specially, the near-wall behavior of the Reynolds stress is well captured although the model predicts a little higher maximum value. It is interesting to note that while $<u'^2>$ and $<v'^2>$ are overpredicted and underpredicted,

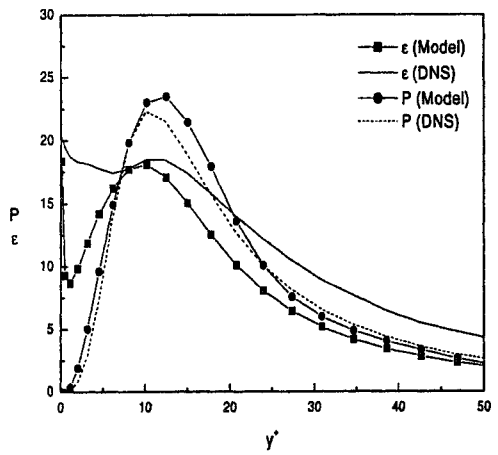

Fig. 6 Turbulent dissipation rate and production

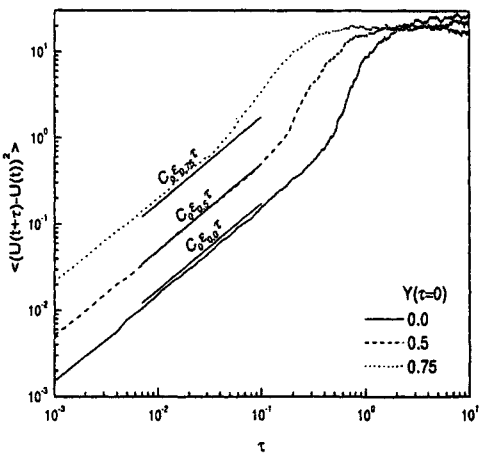

Fig. 7 The Lagrangian velocity structure function for three initial wall-normal locations in the channel

respectively, $<u'v'>$ is relatively well predicted.

Finally, turbulent energy production, $P(=-<u'v'>\frac{d<u>}{dy})$, and dissipation rate are demonstrated in Fig. 6. Our model for ϵ (Eqs. (14), (15)) does not guarantee a nonvanishing value of ϵ near the wall if k behaves correctly, $k \propto y^2$, since $l \propto y^2$ near the wall, where y is distance from the wall. However, the result shows a finite value of ϵ near the wall, suggesting that k scales with $y^{4/3}$, which is confirmed numerically (see Fig. 2). This serves as an example that a model combined with finite property sets the near-wall behavior of one of model element. Although the model produces relatively reasonable value at the wall, the near-wall($0<y^+<10$) behavior shows a large discrepancy compared to the DNS result. Since the Reynolds stress is relatively well predicted, the agreement in turbulent energy production between our model and DNS result is excellent.

4.2 Local performances

In this section, we examine the model's performance in terms of short time behavior. Specially, we focus on the viscous time scale performance. We investigate the Lagrangian velocity structure function, velocity correlation coefficient, dispersion and probability density function which can be predicted with are of accuracy. Although the channel flow is highly anisotropic, local behavior should not deviate much from isotropic characteristics. The Lagrangian velocity structure function (defined by Eq. (1)) from three different initial particle locations, y=0.0(channel center), 0.5, 0.75, is shown in Fig. 7. As shown in Fig. 7, the short time behavior follows the scaling relation derived from Kolmogorov's assumption for the inertial range. According to Kolmogorov's scaling argument for viscous time scale, however, the velocity structure function should be (Monin & Yaglom 1975),

$$D_L(\tau)=\alpha\epsilon^{-3/2}\nu^{-1/2}\tau^2 \quad \text{when } \tau \ll \tau_\eta \qquad (23)$$

where α is a universal constant. Such a quadratic behavior in the viscous dissipation range (τ_η=0.03~0.1 for 3 locations shown in Fig. 7) is not observed in our results. Although we include viscous effects by adding a random Gaussian walk to a particle's position calculation, such a modification does not guarantee a correct scaling property of velocity in the viscous dissipation range. This result can be understood by examining the governing equation for the Lagrangian velocity increment(Eq. (13)). Even with the viscous terms, the model represents a Markov process. As $dt \to 0$, the acceleration due to the last term, $\sqrt{C_0\epsilon}\,dW$, becomes unbounded since $dW \propto \sqrt{dt}$. This Markovian property prevents a smooth variation of velocity, thus the inertial range scaling holds down to the viscous dissipation range and a correct scaling for the viscous dissipation

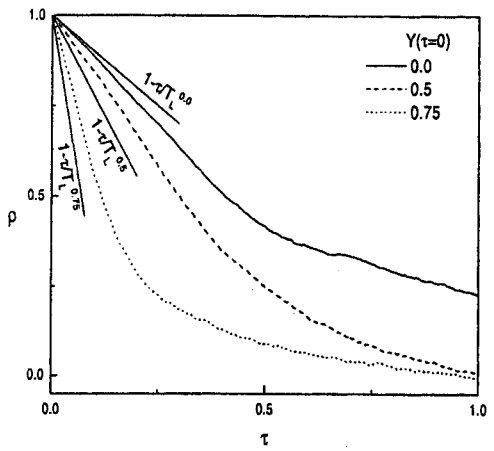

Fig. 8 The Lagrangian velocity correlation coefficient distribution for three initial wall-normal locations

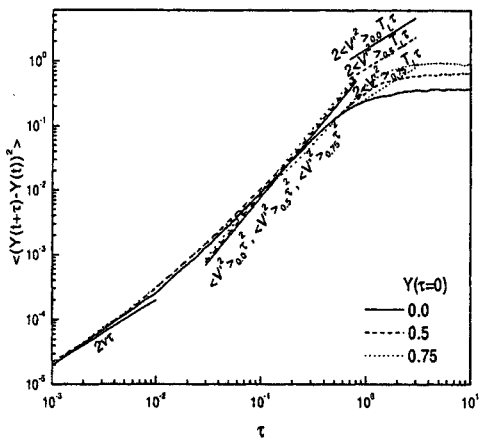

Fig. 9 Mean squared wall-normal dispersion for three initial wall-normal locations

range is not captured. For an exact treatment in the viscous range, a model for the acceleration increment might be necessary, which is believed to guarantee a smooth variation of velocity (see Sawford 1991).

The effect of viscosity is also examined in the Lagrangian velocity correlation. The correlation coefficient defined as:

$$\rho=\frac{<U(t)U(t+\tau)>}{<U(t)^2)} \tag{24}$$

is shown in Fig. 8 for three different initial locations. As in the structure function, the viscous effect is not captured in the correlation coefficient. The slope of the correlation coefficient at $\tau=0$ does not vanish; instead, it has slope of $-1/T_L$ which was defined in Eq. (5). This slope relation is derived from inertial range scaling. The local values of k and ϵ at $\tau=0$ are used in the calculation of T_L in Fig. 8. Results at $y=0.5$, 0.75 show a little deviation which is due to the steep variation of k or ϵ near the wall. This again confirms that the Lagrangian velocity follows inertial range scaling even in the viscous dissipation range. This seems to be a limitation of the present model in simulating viscous effects.

The viscous effect is well represented in a particle's dispersion in the wall-normal direction. Mean-squared dispersion in the wall-normal direction for three different initial locations is shown in Fig. 9. For comparison, the scaling relations for viscous dissipation range, inertial range and long-time limit for isotropic turbulence are shown together. Those are,

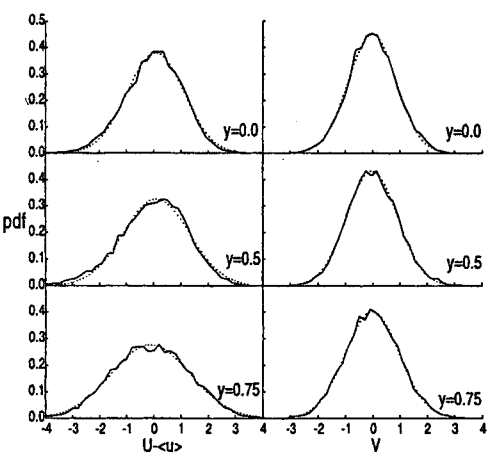

Fig. 10 Probability density functions for the streamwise and wall-normal velocity fluctuations at three wall-normal locations

$$<(Y(t+\tau)-Y(t))^2>$$
$$=2\nu\tau \quad \text{when } \tau\ll\tau_\eta \tag{25}$$
$$=<v'^2>\tau^2 \quad \text{when } \tau_\eta\ll\tau\ll T_L \tag{26}$$
$$=2<v'^2>T_L\tau \quad \text{when } T_L\ll\tau \tag{27}$$

where Eq. (25) is due to Brownian motion and Eqs. (25, 27) are Taylor's formula for isotropic turbulence (Taylor 1921). Since particles strike the wall during the course, long-time limits are not observed and plateau distributions are obser-

ved instead. Commonly, the scaling relation for viscous range is well captured. For inertial range, however, they are mildly represented due to the presence of the walls.

Probability density functions of velocity fluctuation are investigated at three locations in Fig. 10. The pdf of the streamwise velocity fluctuation slightly deviates from normal distribution which has a zero mean and the same variance. Specially, the tail part of the pdf shows an asymmetric distribution. It has a negative skewness and similar behavior was observed in a recent turbulent b. l. experiment (Tsuji & Nakamura 1999). The pdf of the wall-normal component, however, is very close to normal distribution. The pdf of the spanwise component shows the same normal distribution(figure not shown).

5. Conclusion

We developed a numerical algorithm to solve the simple Langevin equation for Lagrangian velocity increment that was derived from Kolmogorov's scaling relation. Viscous effects were also incorporated into the model by adding Brownian random walk model to particles position calculation. For imposition of no-slip condition at the wall, we tested several treatments for the velocity of particles which strike the wall and found that the second-order Taylor expansion is necessary to produce a near-wall particle velocity which is consistent with near-wall mean velocity.

We have investigated the model's performance by applying it to a fully developed turbulent channel flow at a low Reynolds number. A simple near-wall model is adopted for the turbulent dissipation rate. For a few selected empirical constants, the model performs relatively well. The mean velocity in the streamwise direction is underpredicted. Anisotropic nature of turbulence intensities near the wall was not correctly captured, while the Reynolds shear stress distribution was well predicted. a finite value of the dissipation rate at the wall is captured, but the dissipation rate is underpredicted in the region very close to the wall.

We have also examined the model's performance viscous time scale. Assumed scaling relations for inertial range were confirmed, but the scaling relation for viscous dissipation range was confirmed only in dispersion characteristics, and not in velocity. Also, the predided asymmetric distribution of pdf for the streamwise velocity fluctuation near the wall compared very well with an available experimental result.

Considering the simplicity of the model with a minimum number of empirical constants, the current Lagrangian model performs well. This might be due to the model's Lagrangian property; it eliminates uncertainty associated with the closure problem in turbulence modeling. Overall, however, performance of the model is not satisfactory. The present model is not a complete model in the sense that only the Lagrangian property is used to its full extent, while the other part of the model is simplified. We may be able to improve the model for turbulent dissipation rate and velocity in order to include the effect of the near-wall anisotropy. Another point should be made about inclusion of viscous effects. The current incorporation of viscous effects is incomplete since the model cannot demonstrate correct viscous-time scale properties. Much effort should be made to develop a new model to overcome the limitations of the current model.

References

Chorin, A. J., 1973, "Numerical Study of Slightly Viscous Flow," *Journal of Fluid Mechanics,* Vol. 57, pp. 785~796.

Dreeben, T. D. and Pope, S. B., 1997, "Wall-Function Treatment in PDF Methods for Turbulent Flows," *Physics of Fluids,* Vol. 9, p. 2692.

Dreeben, T. D. and Pope, S. B., 1998, "Probability Density Function/Monte Carlo Simulation of Near-Wall Turbulent Flows," *Journal of Fluid Mechanics,* Vol. 357, pp. 141~166.

Durbin, P. A., 1993, "A Reynolds-Stress Model for Near-Wall Turbulence," *Journal of Fluid Mechanics,* Vol. 249, pp. 465~498.

Gardiner, C. W., 1997, *Handbook of Stochastic Methods,,* 2nd edition, Springer-Verlag.

Hardle, W., 1990, *Nonparametric Regression,*

Cambridge University Press.

Howarth, D. C. and Pope, S. B., 1986, "A PDF Modeling Study of Self~Similar Turbulent Shear Flows," *Physics of Fluids,* Vol. 30, No. 4, pp. 1026~1044.

Karatzas, I. and Shreve, S. E., 1991, *Brownian Motion and Stochastic Calculus,* 2nd edition, Springer-Verlag.

Kim, J., Moin, P. and Moser, R., 1987, "Turbulence Statistics in Fully-Developed Channel Flow at Low Reynolds Number," *Journal of Fluid Mechanics,* Vol. 177, p. 133.

Lee, C., Kim, J., Babcock, D. and Goodman, R., 1997, "Application of Neural Networks to Turbulence Control for Drag Reduction," *Physics of Fluids,* Vol. 9, No. 6, pp. 1740~1747.

Minier, J. -P. and Pozorski, J., 1997, "Derivation of a PDF Model for Turbulent Flows Based on Principles from Statistical Physics," *Physics of Fluids,* Vol. 9, No. 6, pp. 1748~1753.

Minier, J. -P. and Pozorski, J., 1999, "Wall-Boundary Conditions in Probability Density Function Methods and Application to a Turbulent Channel Flow," *Physics of Fluids,* Vol. 11, No. 9, pp. 2632~2644.

Monin, A. S. and Yaglom, A. M., 1975, *Statistical Fluid Mechanics: Mechanics of Turbulence*, Vol. 2, p. 359.

Pope, S. B., 1985, "PDF Methods for Turbulent Reactive Flows," *Progress in Energy and Combustion Sciences,* Vol. 11, pp. 119~192.

Pope, S. B., 1994, "Lagrangian PDF Methods for Turbulent Flows," *Annual Review of Fluid Mechanics,* Vol. 26, pp. 23~63.

Pope, S. B. and Chen, Y. L., 1990, "The Velocity-Dissipation Probability Density Function Model for Turbulent Flows," *Physics of Fluids A,* Vol. 2, No. 8, pp. 1437~1449.

Sawford, B. L., 1991, "Reynolds Number Effects in Lagrangian Stochastic Models of Turbulent Dispersion," *Physics of Fluids A,* Vol. 3, pp. 1577~1586.

Taylor, G. I., 1921, "Diffusion by Continuous Movements," *Proc. London Math. Soc.,* Vol. 20, pp. 196~212.

Tsuji, Y. and Nakamura, I., 1999, "Probability Density Function in the Log-Law Region of Low Reynolds Number Turbulent Boundary Layer," *Physics of Fluids,* Vol. 11, No. 3, pp. 647~658.

van Dop, H., Nieuwstadt, F. T. M. and Hunt, J. C. R., 1985, "Random Walk Models for Particle Displacements in Inhomogeneous Unsteady Turbulent Flows," *Physics of Fluids,* Vol. 28, No. 6, pp. 1639~1653.

Appendix

A.1 Integration Scheme

Equation (16) is rewritten as follows:

$$df(t)=a(t)fdt+g(t)dt+h(t,\ f)dW \quad (28)$$

where dependence on the space coordinates is dropped for simplicity. The coefficient $a(t)$ of the first term is proportional to ϵ/k, and near the wall this coefficient becomes unbounded since the turbulent kinetic energy has a limiting value of zero while the dissipation rate has a nonzero value at the wall. An explicit integration of this term can cause numerical instability. To avoid this, an exact integration method is adopted. With a low-storage 3rd-order Runge-Kutta scheme, an integration scheme for each substep in one time step reads,

$$f^{n+k/3}=\exp((\alpha_k+\beta_k)\Delta t a^{n+(k-1)/3})\\ [f^{n+(k-1)/3}+\alpha_k\Delta t g^{n+(k-1)/3}\\ +\beta_k\Delta t g^{n+(k-2)/3}+h^{n+(k-1)/3}\Delta W^{k/3}] \quad (29)$$

where n and k denote n-th time step and substep varying from 1 to 3, respectively. Discretized Wiener process is given as:

$$\Delta W^{k/3}=\mathrm{N}(0,\ (\alpha_k+\beta_k)\Delta t) \quad (30)$$

where $\mathrm{N}(A,\ B)$ denotes a random number selected from a normal Gaussian distribution with mean A and variance B. The coefficients are, $\alpha_1=8/15$, $\alpha_2=5/12$, $\alpha_3=3/4$, $\beta_1=0$, $\beta_2=-17/60$, $\beta_3=-5/12$, respectively. Also, there is no restriction on the time step.

A.2 Kernel Regression

Suppose that statistical data $(y_j,\ f_j)$ with $j=1,\ \cdots,\ J$ are given. A good approximate function $\tilde{f}(y)$ is sought such that the error associated with the approximation is minimized. The error is defined as:

$$Error=\sum_{j=1}^{J}K_h(y-y_j)(f_j-\tilde{f}(y-y_j))^2 \quad (31)$$

where $K_h(y)$ is a kernel function. In our study, we chose the following kernel function:

$$K_h(y)=\frac{3}{4}\left(1-\frac{y^2}{h^2}\right) \text{ when } |y/h|<1 \quad (32)$$

$$=0 \quad \textit{otherwise} \quad (33)$$

A polynomial fitting function is selected:

$$\tilde{f}(y)=\sum_{k=0}^{K}c_k y^k. \quad (34)$$

From this, derivatives of up to K-th order at the point of kernel center, $y=0$, can be obtained,

$$\frac{d^m\tilde{f}}{dy^m}=m!\,c_m. \quad (35)$$

The coefficients c_k are obtained by solving the following matrix equation derived from the error minimization condition:

$$Y_{ij}c_j=F_i \quad (36)$$

with $i, j=0, \cdots, K\text{-}1$. Y_{ij} and F_i are given as:

$$Y_{ij}=\sum_{l=1}^{J}K_h(y-y_l)(y-y_l)^{i+j} \quad (37)$$

$$F_i=\sum_{l=1}^{J}K_h(y-y_l)f_l(y-y_l)^i \quad (38)$$

K is chosen as 3 and the parameter h of the kernel function is computed at every time step such that the number of selected data are maintained constant. Near the boundary, where data are asymmetrically distributed, a physical condition is imposed by adding ghost data with appropriate function values at the boundary. For example, velocity and turbulent kinetic energy vanish there; therefore, added data have zero function values.